PHYSICAL REVIEW D VOLUME 47, NUMBER 3 1 FEBRUARY 1993

Charged Higgs bosons at the Superconducting Super Collider

R. Michael Barnett
Lawrence Berkeley Laboratory, Berkeley, California 94720

Ray Cruz and John F. Gunion
Department of Physics, University of California, Davis, California 95616

Bradley Hubbard
Santa Cruz Institute for Particle Physics, University of California, Santa Cruz, California 95064

(Received 26 June 1992)

We study techniques for discovering at the Superconducting Super Collider (SSC) a charged Higgs boson of a two-doublet Higgs sector in the decay $t \to H^+ b$, for a variety of top-quark and charged-Higgs-boson masses. $t\bar{t}$ events are selected by demanding a high-p_T lepton and a tagged b jet. One technique is to search for an excess of τ leptons from H^+ decays. For $\tan\beta \equiv v_2/v_1 \gtrsim 0.5$, this technique is usually viable, even for a fraction of the expected SSC yearly luminosity (depending upon m_t and m_{H^+}). Techniques for approximately determining the H^+ mass in this mode are discussed. We also demonstrate that for $0.1 \lesssim \tan\beta \lesssim 1.5$ a peak in the two-jet mass distribution resulting from $H^+ \to c\bar{s}$ can be found, and a precise H^+ mass determination is possible even in a fraction of an SSC year, provided $B(t \to H^+ b)$ is not too small.

PACS number(s): 14.80.Gt, 13.20.Jf, 13.85.Qk, 13.87.Ce

I. INTRODUCTION

One of the most attractive extensions of the standard Higgs sector contains two Higgs doublets and, consequently, both charged and neutral physical Higgs bosons [1]. If the charged Higgs boson is lighter than the top quark, then the branching ratio for the decay $t \to H^+ b$ could be comparable to that for $t \to W^+ b$. Since the Superconducting Super Collider (SSC) [and the CERN Large Hadron Collider (LHC)] provide very high rates of top-quark production, detailed studies of t decays are possible, providing a significant opportunity for detection of the $t \to H^+ b$ decays. An early discussion of the phenomenology of such a situation, and the relevant tree-level branching ratios, appeared in Ref. [1]. The present work is an extension of the detailed study by the Solenoidal Detector Collaboration (SDC) [2]. (See also Ref. [3].) Related work in the context of other experiments has appeared in Refs. [4–6].

The top-quark and charged-Higgs-boson branching fractions depend upon the couplings of the two Higgs doublets to the quarks and leptons. There are two possible models normally considered for these couplings that are consistent with the absence of flavor-changing neutral currents. In one model (model II in the notation of Ref. [1]) the neutral component of one of the doublets is responsible for generating the mass of leptons and charge $-\frac{1}{3}$ quarks, while the other generates the mass of charge $\frac{2}{3}$ quarks. This is the model predicted by minimal supersymmetry and will be the one upon which we primarily focus.[1] The couplings of the charged Higgs bosons to fermions are entirely determined by the quark and/or lepton masses and by $\tan\beta = v_2/v_1$, where v_1 (v_2) is the vacuum expectation value of the Higgs field which couples to the down- (up-) type fermions. Therefore, if we assume that the decays $H^+ \to W^+ H_i$ ($H_{1,2}$ being the CP-even Higgs scalars) are kinematically forbidden,[2] $\tan\beta$ determines the branching fractions for $t \to bH^+$, $H^+ \to \tau\nu$, and $H^+ \to c\bar{s}$.

The predicted branching ratios for the various $H^\pm$ decay modes as a function of the parameter $\tan\beta$ are shown in Fig. 1. The results shown are essentially independent of $m_{H^\pm}$.[3] Results for $B(t \to H^+ b)$ are given in Fig. 2 for various top-quark and charged-Higgs-boson mass choices.[4] The current limit on the charged-Higgs-boson mass from the CERN e^+e^- collider LEP is $m_{H^+} > 41.7$ GeV at the 95% confidence level; the 95% confidence-level limit on the top-quark mass obtained without assuming dominance of the $t \to W^+ b$ decay is $m_t > 55$ GeV [7].

Theory provides some prejudices concerning the likely value of $\tan\beta$. Renormalization-group analysis in the context of a typical grand unification scheme leads to a correct pattern of symmetry breaking with large m_t only if $\tan\beta$ is greater than 1 [1]. In addition, very small values of $\tan\beta$ ($\lesssim 0.2$) would place the $H^+ \to t\bar{b}$ coupling in a nonperturbative regime for $m_t \gtrsim 200$ GeV.

From Fig. 1 we see that $H^+ \to \tau^+ \nu$ is the dominant de-

[1]We shall, however, remark on the alterations in branching ratios and search strategies that would be required in model I, in which one of the Higgs-doublet fields couples to all quarks and leptons, and the other Higgs field does not couple to any matter fields.

[2]Should such decays be kinematically allowed, they are very likely to dominate, and our detection strategies for the H^+ would be very different.

[3]In model I, the $H^+ \to cs, cb, \tau\nu$ branching ratios are all constant at 0.63, 0.015, and 0.355, respectively.

[4]In model I, the $t \to H^+ b$ branching ratio falls rapidly once $\tan\beta$ increases beyond about 1, implying that all detection modes will become difficult beyond $\tan\beta \sim 4$.

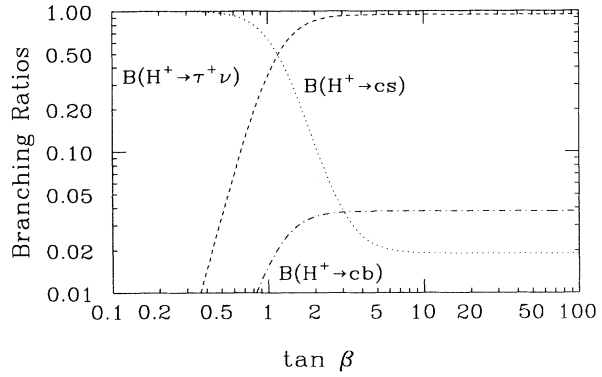

FIG. 1. Branching fractions for $H^+ \to \tau\nu$, $c\bar{s}$, $c\bar{b}$ as a function of tanβ, using the model II formulas of Ref. [1]. Results are essentially independent of $m_{H^\pm}$. We take $m_b = 4.7$ GeV, $m_c = 1.4$ GeV, and $m_s = 0.15$ GeV.

cay mode in the preferred tan$\beta \gtrsim 1$ region. As tanβ approaches 6, the t branching fraction to $H^\pm$ drops to a minimum, while the $H^\pm \to \tau\nu$ branching ratio approaches unity. For smaller values of tanβ the $\tau\nu$ branching ratio is quite small, and the $c\bar{s}$ mode will provide the best hope for $H^\pm$ detection.

We have investigated two methods for $H^\pm$ detection in $t\bar{t}$ events. The first is based on searching for an excess of τ leptons. This technique is most effective for tan$\beta \gtrsim 0.5$ (where the branching ratio of $H^+ \to \tau\nu$ is large). The other method is to reconstruct the hadronic decays $H^+ \to c\bar{s}$; it is useful for smaller values of tanβ where $t \to H^+ b$ and $H^+ \to c\bar{s}$ are both large. In each case, events are triggered by requiring one t quark to decay via $t \to bW \to bl\nu$, yielding an isolated electron or muon (l) with $p_T > 40$ GeV/c and $|\eta| < 2.5$. The isolation requirement used was that the energy (excluding that of the lepton) within a cone of radius $\Delta R \equiv \sqrt{\Delta\eta^2 + \Delta\phi^2} = 0.4$ about the lepton be less than 25% of the lepton momentum. The results do not depend critically on the precise isolation criterion. An example (for $m_t = 250$ GeV) of the results for the ratio of lepton track momentum to the total energy within the cone of 0.4 appeared in Ref. [2]. The lepton isolation spectrum and resulting efficiency for isolation do not depend very strongly on the top-quark mass. We assume an efficiency for identifying electrons and muons of 85%, once they have satisfied our p_T and $|\eta|$ cuts.

The events are further selected by requiring a tagged b jet[5] (from the decay of the t or $\bar{t}$) with $p_T > 30$ GeV within $|\eta| < 2.0$. A b jet can be tagged either through a semi-isolated lepton from the b decay [8], or via a secondary vertex. The efficiency for tagging the b jets through secondary vertices is discussed in Ref. [9]. For the b jet cuts given above, a full detector simulation yields an efficiency of 0.30/b jet for tagging a secondary vertex; it is estimated that this would increase to ~ 0.35 if leptonic tags are included. The non-$t\bar{t}$ background coming from $Wb\bar{b}$, $Wc\bar{c}$, $Wc\bar{b}$, and $Wb\bar{c}$ final states, and satisfying the above criteria, has been computed and is small even before the $H^\pm$ signal criteria are implemented. Backgrounds from $b\bar{b}$ +jets and $c\bar{c}$ +jets are also negligible. Even though the uncut cross sections for these latter processes are several orders of magnitude larger than the $t\bar{t}$ cross section, by the time all cuts and isolation requirements are imposed these backgrounds are negligible compared to the signal. Isolation requirements are particularly powerful: for example, as studied in the SDC Technical Design Report (TDR) (Ref. [3], Table 3.6), implementation of the lepton isolation requirement on a $p_T > 40$ GeV/c lepton from b or c semileptonic decay results in a suppression factor of at least 200. Further suppression of such backgrounds arises by virtue of cuts, discussed later, which are employed to identify the $H^+ \to \tau^+\nu$ or $H^+ \to c\bar{s}$ decays. Thus, there are no significant non-$t\bar{t}$ backgrounds to the events of interest when a tagged b jet is required.

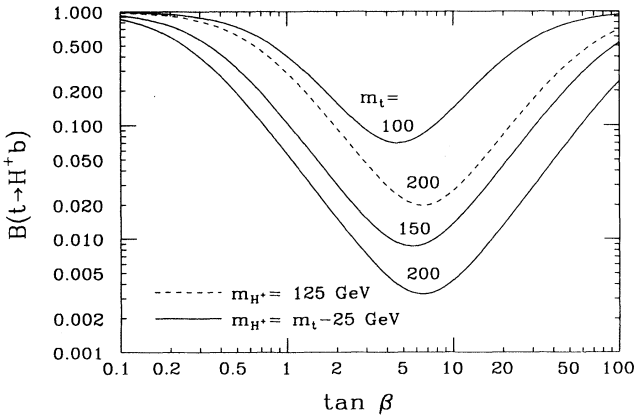

FIG. 2. Branching ratios for $t \to H^+ b$ as a function of tanβ for a variety of top-quark and charged-Higgs-boson masses. Solid curves indicate results obtained for $m_t = 100$, 150, and 200 GeV with $m_{H^+} = m_t - 25$ GeV. The dashed curve gives $B(t \to H^+ b)$ for $m_t = 200$ GeV and $m_{H^+} = 125$ GeV.

II. METHOD 1: SEARCH FOR $H^+ \to \tau\nu$

In method 1 we search for l-τ events (e.g., $t \to bW^+ \to bl^+\nu$, $\bar{t} \to \bar{b}H^-$, or $\bar{b}W^- \to \bar{b}\tau^-\nu$) in which the τ decays to a single $\pi^\pm$ (or $K^\pm$) with $p_T > p_T^{\rm cut}$ ($p_T^{\rm cut} = 50$ or 100 GeV). We do this for two reasons. First, the signature of a very hard isolated pion from $\tau^+ \to \pi^+\nu$ (or $K^+\nu$) is distinctive; this signature is an isolated charged hadron whose momentum (from tracking) and energy (from calorimetry) agree within errors. The isolation requirement used was that the energy (excluding that of the pion), within a cone of radius $\Delta R = 0.4$ about the pion, be less than 25% of the pion momentum. (Or, equivalently, the pion must carry more than 80% of the total energy found within the cone.) The probability for a

[5]We shall later discuss the increased significance of the charged Higgs signal that would occur in the absence of any b-tagging requirement (though this would require that backgrounds eliminated by b tagging remain small).

QCD jet with $p_T > 50$ GeV to satisfy this requirement is less than 0.1% [10]. For one-prong τ candidates produced via H^+ decays, the distribution of the ratio of pion track momentum to the total energy within a cone of 0.4 is given in Fig. 3 for the sample case of $m_t = 150$ GeV, $m_{H^+} = 125$ GeV. As discussed below, this distribution is sensitive to whether the τ candidate arises from H^+ vs W^+ decays, as well as the H^+ mass in the first case.

The second reason for using the single π decay of the τ is that the spectrum for the π from a τ that originates from the $H^\pm$ is much harder than for a π from a τ which originates from a $W^\pm$. Since the coupling of W to $\tau\nu$ conserves chirality and the ν are left handed, the τ^- (τ^+) are left (right) handed (up to corrections of order m_τ/m_W). In contrast, as first emphasized in Ref. [2], the $\tau^\pm$ from the decay of $H^\pm$ would have the opposite polarizations, since the $H^\pm$ is a scalar and its couplings maximally violate chirality; as in Ref. [2], we shall employ this difference in polarizations of the τ in order to enhance the signal for the charged Higgs boson [11]. In W decays, the τ polarization results in the preferred direction for emission of the $\pi^\pm$ being opposite the momentum of the τ. In $H^\pm$ decays, since the $\tau^\pm$ has the opposite polarization, the $\pi^\pm$ tends to be emitted parallel to the τ momentum. Consequently, the p_T spectrum of the isolated pion from the charged Higgs decay is shifted to higher p_T. Furthermore, for any choice of charged-Higgs-boson mass such that $m_{H^\pm}$ is significantly larger than m_W, the p_T of τ's from the $H^\pm$ decay will already be larger on average than that from W decay. These effects will enhance the $H^\pm$ signal over the $W^\pm$ background. Since a π from W^+ decay is softer than that from H^+ decay, not only will it have a smaller probability of passing a given $p_T(\pi)$ cut, but also it will be less isolated in the sense that it will be less likely to pass the $p_T(\pi)/E_T(\text{cone}) > 0.8$ isolation cut. In short, polarization correlations and kinematic effects both enhance the relative number of events containing a $H^\pm$.

Our study was performed using the ISAJET 6.31 Monte Carlo program, including a modification to produce the correct τ polarization in the decays of $W^\pm$ and $H^\pm$. Implementation of the correct polarization correlations for the t-quark decay chain is crucial in obtaining an accurate result. The detector response was simulated by smearing the produced energy and momenta with the assumed calorimeter and tracking resolutions [12]. Multiple-event pileup was not simulated, since it is not expected to affect our results at the nominal SSC luminosity. The main effect of multiple events would be to decrease slightly the efficiencies for observing isolated leptons and τ's, but this should be a small effect for the p_T thresholds used in this study.

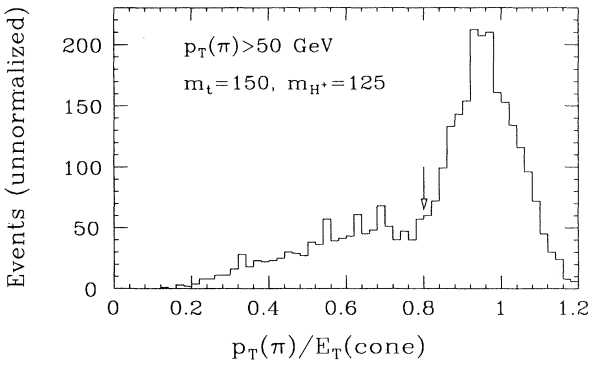

FIG. 3. The ratio of measured single-track momentum to energy within a cone of radius $R \equiv \sqrt{(\Delta\eta)^2+(\Delta\phi)^2} = 0.4$ for pions from the decay of τ's in $H^+ \to \tau^+\nu$. The arrow indicates the cut adopted.

A. Universality argument in the search for $H^+ \to \tau\nu$

The most sensitive means of detecting the presence of a charged Higgs boson decaying to τ's is to employ lepton universality in W decays. If t quarks decay only to W^+b, then the observed number N_{ll} of l^+-l^- events plus lepton universality in W decays allows us to compute the number $N_{l\tau}$ of l-τ events expected:

$$N_{l\tau} = 2N_{ll}\frac{B(W\to\tau\nu)e_{l\tau}}{B(W\to l\nu)e_{ll}} , \tag{1}$$

where e_{ll} and $e_{l\tau}$ are the overall efficiencies for detecting the two different types of events,[6] and $B(W\to l\nu) \equiv B(W\to e\nu)+B(W\to\mu\nu)$. In Eq. (1) the factor of 2 is due to either W being able to decay to τ. Assuming that $B_W \equiv B(t\to W^+b) = 100\%$, N_{ll} is related to the number of $t\bar{t}$ events ($N_{t\bar{t}}$) by

$$N_{ll} = N_{t\bar{t}}B^2(W\to l\nu)e_{ll} , \tag{2}$$

and the actual number of l-τ events observed would be

$$N_{l\tau} = 2N_{t\bar{t}}B(W\to l\nu)B(W\to\tau\nu)e_{l\tau} = N_{ll}\frac{e_{l\tau}}{e_{ll}} , \tag{3}$$

where the factor of 2 arises since either W can decay to the τ.

If top quarks can decay to H^+b as well as to W^+b, then we consider $W^+W^-b\bar{b}$, $W^\pm H^\mp b\bar{b}$, and $H^+H^-b\bar{b}$ final states, so that the number of observed l-τ events would be

$$N_{l\tau} = N_{l\tau}^{WW} + N_{l\tau}^{WH} + N_{l\tau}^{HH} \tag{4}$$

(the mixture depends on the branching ratio B_H). The contribution from $H^+H^-b\bar{b}$ final states, $N_{l\tau}^{HH}$, can be ignored because the lepton trigger then requires $H\to\tau\nu\to l\nu\bar{\nu}$, but, in the range where $t\to bH^+$ is large, the branching ratio $B(H^+\to\tau\nu)$ (and consequently the lepton trigger efficiency) is very small.

The preference for H^+ to decay to $\tau\nu$ rather than $e\nu$ or $\mu\nu$ implies that an excess of l-τ events over the universali-

[6]Of course, determination of these efficiencies requires a Monte Carlo computation of the efficiency for triggering on the leptons and for whatever other cuts may be appropriate. In the case of e_{ll}, the necessary studies have been done elsewhere [3] and are not described here. $e_{l\tau}$ will be discussed in detail shortly.

ty prediction would be detected. Not only are l-τ events enhanced, but l^+-l^- events are depleted. In this procedure, one first employs l-l events[7] to determine the number $N_{t\bar{t}}$ of $t\bar{t}$ events as a function of $B_H \equiv B(t \to H^+ b) = 1 - B_W$ using

$$N_{ll} = N_{t\bar{t}}(1-B_H)^2 B^2(W \to l\nu) e_{ll} \ . \tag{5}$$

Again, τ's from H decays are not an important source of l's because, for tanβ values where $B(t \to H^+ b)$ is large, $B(H^+ \to \tau\nu)$ is small.

When B_H is nonzero, the prediction of universality, [Eq. (3)] for the number of detected l-τ events originating in $t\bar{t} \to W^+ W^- b\bar{b}$ must be modified by inserting $(1-B_H)^2$, yielding

$$N_{l\tau}^{WW} = 2(1-B_H)^2 N_{t\bar{t}} B(W \to l\nu) B(W \to \tau\nu) e_{l\tau} = N_{ll} \frac{e_{l\tau}}{e_{ll}} \ , \tag{6}$$

where N_{ll} is given in Eq. (5). Similarly, for $t\bar{t} \to W^\pm H^\mp b\bar{b}$ events,

$$\begin{aligned} N_{l\tau}^{WH} &= 2B_H(1-B_H) N_{t\bar{t}} B(W \to l\nu) B(H \to \tau\nu) e'_{l\tau} \\ &= 2N_{ll} \frac{B_H}{1-B_H} \frac{B(H \to \tau\nu)}{B(W \to l\nu)} \frac{e'_{l\tau}}{e_{ll}} \ , \end{aligned} \tag{7}$$

where the factor of 2 arises from the presence of both $t\bar{t} \to H^+ W^-$ and $t\bar{t} \to W^+ H^-$ events. The efficiency for detecting the l-τ events in the mixed WH decays, $e'_{l\tau}$, will generally be quite different than that for WW events, $e_{l\tau}$. Note that the parameter tanβ of the two-doublet Higgs model enters the above equations via both B_H and $B(H^+ \to \tau\nu)$.

These predictions for $N_{l\tau}^{WW}$ and $N_{l\tau}^{WH}$ are independent of the theoretical calculation of the $t\bar{t}$ cross section. Observation of a violation of universality consists of detecting the $N_{l\tau}^{WH}$ excess events above the number $N_{l\tau}^{WW}$ predicted on the basis of universality. Our ability to do so clearly depends upon the efficiencies appearing in Eqs. (6) and (7), to which we now turn.

B. Formulas ingredients

We now detail the various ingredients required in computing actual numbers of events. In our computations, we assume the branching ratios $B(W \to l\nu)/2 = B(W \to \tau\nu) = \frac{1}{9}$. We shall also use $B(\tau \to \pi\nu) = 11.5\%$. [In practice, one would also include $K\nu$ decays; the current value for $B(\tau \to \pi\nu + K\nu)$ is 12.7% [7]]. In computing the efficiencies in the above formulas, we employ ISAJET, including the earlier-described modification. ISAJET yields the standard QCD predictions for $N_{t\bar{t}}$. At SSC energies, we have $N_{t\bar{t}} = 4.2\times10^8$, 1.1×10^8, 3.6×10^7, and 1.5×10^7 events/SSC year ($\int \mathcal{L}\, dt = 10^4$ pb^{-1}) for $m_t = 100$, 150, 200, and 250 GeV, respectively.

The efficiencies $e_{l\tau}$ (for WW events) and $e'_{l\tau}$ (for WH events) are determined by our procedure for tagging and isolating the l-τ events of interest. As outlined earlier, we first tag a lepton for the W (efficiency e_l); then we tag a b-quark jet coming from either t decay (efficiency e_b); and finally we tag a fast isolated pion coming from the $\tau \to \pi\nu$ decay [efficiency $B(\tau \to \pi\nu) e_\pi$]. These latter two efficiencies are conditional: e_b is computed given that the l has already been tagged, and e_π is obtained assuming that both the l and the b have been tagged. All these efficiencies include the effects of the p_T and η cuts specified earlier, and in the case of e_l and e_π, the efficiency for achieving the given isolation criteria. We thus have

$$e_{l\tau} = B(\tau \to \pi\nu) e_l e_b e_\pi \ , \tag{8}$$

and similarly for $e'_{l\tau}$. For given choices of the various p_T and η cuts, etc., the efficiencies e_l, e_b, and e_π can depend on m_t and $m_{H^\pm}$.

The efficiencies for the various cases that we consider in this paper are given in Table I. Several features of these efficiencies are noteworthy. First, in practice, we find that, for the lepton-tagging cuts specified earlier, e_l depends solely on m_t. Regarding e_b, we see that it depends relatively weakly on the H^+ mass choice. This occurs, in part, because many of the tagged b jets are associated with the $t \to Wb \to l\nu b$ side of the event. The slow decrease of e_b with increasing $m_{H^\pm}$ is a consequence of the increasingly soft spectrum of the b quark on the $t \to H^+ b$ side of the event. This is illustrated in Fig. 4, where we compare the p_T spectrum of the b jet from $t \to W^+ b$ to the p_T spectrum of the b jet from $t \to H^+ b$.

TABLE I. The efficiencies for lepton triggering, for b tagging [including the $p_T(b)$ cut], and for finding a π from the decay of the τ for the given $p_T(\pi)$ cut (units are GeV). The quoted efficiencies do not include the branching ratios for the t-quark decays. For $m_t = 100$, 150, and 200 GeV, the numbers of events before efficiencies are 4×10^8, 1×10^8, and 4×10^7, respectively.

m_t (GeV)	$t \to W^\pm$ or $H^\pm$ (mass)	e_l	e_b	e_π $p_T(\pi) > 50$	e_π $p_T(\pi) > 100$
100	$W^\pm$	0.35	0.10	0.044	0.0022
100	$H^\pm$ (75)	0.35	0.13	0.16	0.020
100	$H^\pm$ (85)	0.35	0.087	0.18	0.040
100	$H^\pm$ (95)	0.35	0.066	0.27	0.077
150	$W^\pm$	0.39	0.27	0.065	0.011
150	$H^\pm$ (75)	0.39	0.28	0.18	0.043
150	$H^\pm$ (125)	0.39	0.22	0.29	0.090
150	$H^\pm$ (140)	0.39	0.20	0.32	0.12
200	$W^\pm$	0.46	0.31	0.091	0.018
200	$H^\pm$ (125)	0.46	0.30	0.31	0.11
200	$H^\pm$ (175)	0.46	0.26	0.39	0.16

[7] An l in either l^+-l^- or l-τ events can also originate from a leptonic τ decay. This contribution is small because of the combination of the branching ratio and the high-p_T cut on the lepton. Using ISAJET, we find a correction to the predicted l^+-l^- rate from WW of approximately 10% for the $p_T > 40$ GeV lepton cut, and this correction can be determined with high precision.

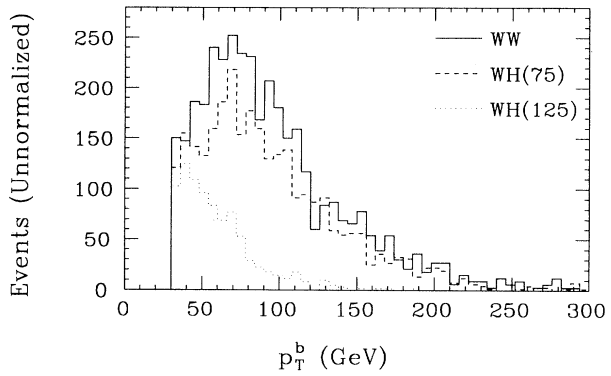

FIG. 4. The p_T spectrum of a tagged b jet from $t \to H^+ b$ is compared to that for $t \to W^+ b$. We plot results for WW, WH with $m_{H^+}=75$ GeV, and WH with $m_{H^+}=125$ GeV. We have taken $m_t=150$ GeV. The normalizations of the different spectra have been chosen so as to best illustrate the shape differences. The true spectrum for the b associated with the $\tau\nu$ side of the event requires combining with appropriate (tanβ-dependent) relative normalizations, the $t \to W^+ b$ spectrum with a $t \to H^+ b$ spectrum. Plots of this type will appear later.

Finally, we see explicitly that, as discussed at the end of the last section, the efficiency e_π for observing the pion or kaon above the p_T cut is substantially higher for the WH cases than for the WW case, for any given choice of m_t.

To illustrate further the importance of the difference between the polarization of the τ in WH vs WW events, we plot in Fig. 5 the $p_T(\pi)$ spectra for $m_t=150$ GeV, comparing results for WW events and WH events. From the $m_{H^\pm}=75$ GeV spectrum we see that the pion spectrum for WH events is shifted to substantially higher $p_T(\pi)$ values compared to WW events, even when the $H^\pm$ and W have comparable masses. This is a direct reflection of the transmission of the τ polarization to the spectrum of the π to which it decays. When $m_{H^\pm}$ is substantially larger than m_W, $p_T(\pi)$ for WH events is shifted to even larger values (see the $M_{H^\pm}=125$ GeV curves),

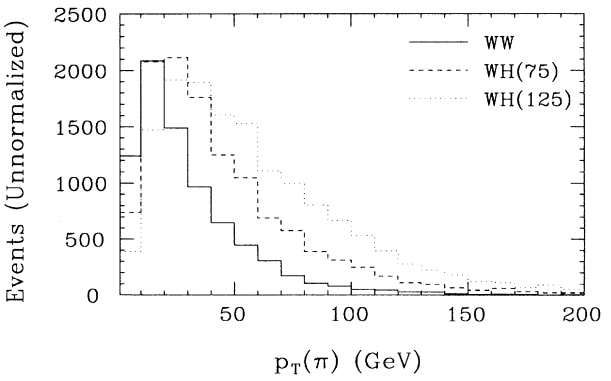

FIG. 5. The $p_T(\pi)$ spectrum for WW events is compared to that for WH events for the choices $m_{H^\pm}=75$ GeV and $m_{H^\pm}=125$ GeV. We have taken $m_t=150$ GeV. A b tag has been required, and an isolation cut of $p_T(\pi)/E_T(\text{cone})>0.8$ on the π has been imposed.

and the resulting efficiency e_π for observing the pion or kaon above a given p_T cut is then even higher, as illustrated in Fig. 6. Note that even for a cut at $p_T(\pi)=0$, the e_π for the H^+ is higher than for the W^+ as a result of the fact (noted earlier) that the π's from the H^+ will, being more energetic on average, tend also to be more isolated.

Of course, in actuality we must combine WW and WH events according to the preceding formulas. The appropriate weighting depends upon tanβ. For illustration, in Fig. 7 we compare the predicted (from universality) and observed p_T spectrum of the isolated pion coming from τ decay for the case tan$\beta \simeq 1.2$ [which yields $B_H \sim 0.075$ and $B(H^+ \to \tau\nu) \sim 0.50$], where the influence of the $H^\pm$ would be large. In this favorable case, the excess due to the $t \to H^+ b$ decays over the universality prediction is more than a factor of 4. Also shown are the predictions for tan$\beta=5.5$, which is the least favorable case ($B_H \sim 0.009$).

C. Results

Let us now quantify the amount of deviation from universality that would be caused by the presence of a charged Higgs boson in t decays. Universality predicts that the number of l-τ events with an isolated single hadron (π^+ or K^+) is just $N_{ll}(e_{l\tau}/e_{ll})=N_{l\tau}^{WW}$, and the observed excess is obviously $N_{l\tau}-N_{l\tau}^{WW}=N_{l\tau}^{WH}$. We can compute the significance of this excess as the number of standard deviations by which the observed number of isolated pions exceeds the prediction from universality:

$$N_{\rm SD}=\frac{N_{l\tau}-N_{ll}e_{l\tau}/e_{ll}}{\sqrt{N_{l\tau}}}=\frac{N_{l\tau}^{WH}}{\sqrt{N_{l\tau}^{WH}+N_{l\tau}^{WW}}} . \tag{9}$$

$N_{\rm SD}$ is a function of the Higgs model parameter tanβ. A sample plot of $N_{\rm SD}$ as a function of M_{H^+} for the particular choices of $m_t=150$ GeV and tan$\beta=5.5$ appears in Fig. 8. Figure 8 illustrates the extent to which a viable signal survives as we approach the kinematic threshold for $t \to H^+ b$ decay.

Results for $N_{\rm SD}$ at other tanβ values (above 0.5) are generally substantially larger. This is illustrated in Fig. 9,

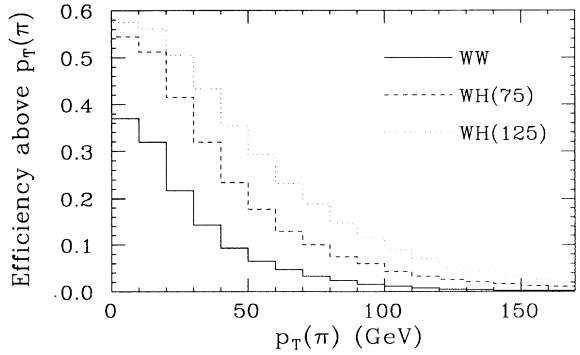

FIG. 6. Efficiency for pions from τ decays to pass a p_T threshold cut in $WWb\bar{b}$ decays and $WHb\bar{b}$ decays. We have taken $m_t=150$ GeV. A b tag has been required, and an isolation cut of $p_T(\pi)/E_T(\text{cone})>0.8$ on the π has been imposed. Results for the $WHb\bar{b}$ case are given for $m_{H^+}=75$ and 125 GeV.

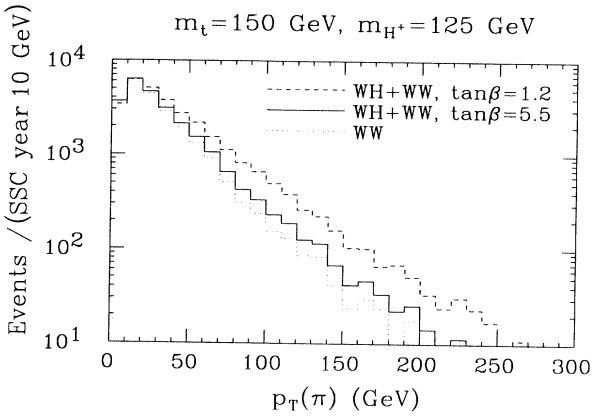

FIG. 7. The transverse momentum distributions for isolated pions coming from $t\bar{t}$ events where $m_t = 150$ GeV. The dotted histogram is the prediction from universality [i.e., corresponding to $N_{l\tau}^{WW}$ in Eq. (6)]. The solid and dashed histograms would be the actual observed spectra if a charged Higgs boson of mass $m_{H^+} = 125$ GeV is present [corresponding to the sum of $N_{l\tau}^{WW}$ and $N_{l\tau}^{WH}$, see Eqs. (6) and (7)]. These figures employ the branching ratios specified for $\tan\beta = 1.2$ and 5.5 in the text. For these plots a b tag is required, and an isolation cut of $p_T(\pi)/E_T(\text{cone}) > 0.8$ on the π has been imposed.

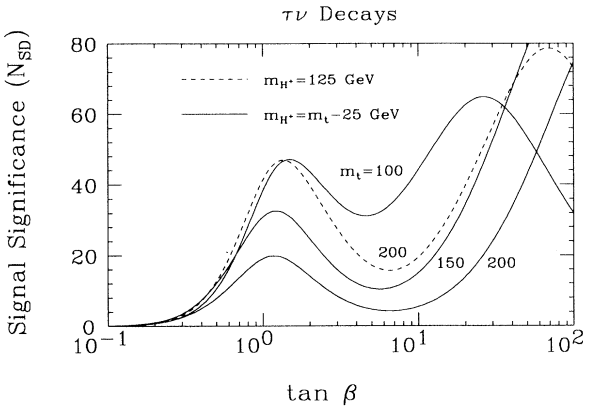

FIG. 9. Statistical significance N_{SD} [see Eq. (9)] of the excess of isolated pions due to $t \to H^+ b$, $H^+ \to \tau\nu$, and $\tau \to \pi\nu$ relative to expectations for $t \to W^+ b$ (assuming lepton universality) as a function of $\tan\beta$. For this figure, we require an isolated lepton with $p_T > 40$ GeV, an isolated pion with $p_T > 100$ GeV, and a single b tag. The dip in N_{SD} is caused by the dip in the $t \to H^+ b$ branching ratio (see Fig. 2). The curves correspond to the various different top-quark and charge-Higgs-boson mass choices considered in Fig. 2. Solid curves indicate results obtained for $m_t = 100$, 150, and 200 GeV with $m_{H^+} = m_t - 25$ GeV. The dashed curve is for $m_t = 200$ GeV and $m_{H^+} = 125$ GeV.

where N_{SD} is plotted for a p_T cut on the isolated pion of 100 GeV (with b tagging). As already detailed, we have employed the efficiencies listed in Table I, as obtained from ISAJET. We remark again that it is critical to keep track of the polarization of the τ's in the Monte Carlo analysis; ignoring the polarization reduces the statistical significance by at least a factor of 2 in most cases. Given the b-tagging requirement, we have estimated that the backgrounds from $Wb\bar{b}$ reduce the number of standard deviations by less than 3%; all other W-jet-jet backgrounds together are smaller than this because the b-jet-tagging requirement more than compensates for the larger production cross sections of some of these channels.

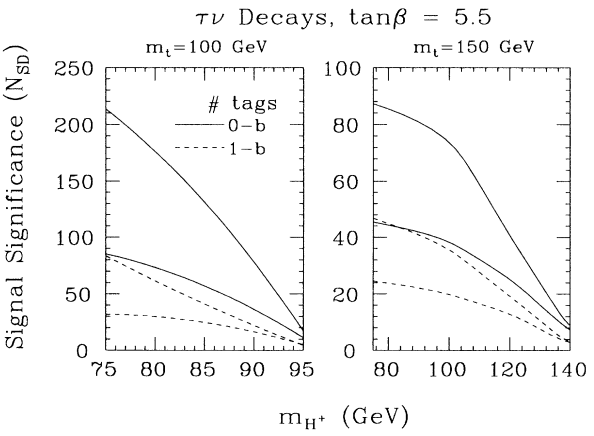

FIG. 8. Statistical significance N_{SD} as a function of $m_{H^\pm}$ for $m_t = 100$ and 150 GeV, with and without a b tag and $p_T(\pi)$ cuts of 50 and 100 GeV (the upper and lower lines for a given b-tag number, respectively). The unfavorable $\tan\beta = 5.5$ value is employed in computing N_{SD}. We have taken $m_b = 4.7$ GeV in our computations.

Requiring 5 standard deviations above background, we conclude that after 1 yr of SSC running we could detect the presence in top decays of the charged Higgs boson decaying to τ's for all $\tan\beta > 0.5$ in almost all cases studied. The only marginal cases among those that we have investigated are $m_t = 100$ GeV, $m_{H^+} \gtrsim 95$ GeV and $m_t = 150$ GeV, $m_{H^+} \gtrsim 140$ GeV. For these m_t, m_{H^+} mass choices, N_{SD} drops somewhat below 5 when $\tan\beta$ is such that $B(t \to H^+ b)$ is near its minimum. For $m_t = 100$ GeV, $m_{H^+} = 95$ GeV, $B(t \to H^+ b)$ reaches a minimum of 2.1×10^{-3} at $\tan\beta \sim 4.7$, at which point we find $N_{SD} \sim 4.7$ when one b tag is required and a cut of $p_T(\pi) > 100$ GeV is imposed. For $m_t = 150$ GeV, $m_{H^+} = 140$ GeV, $B(t \to H^+ b)$ reaches a minimum of 1.7×10^{-3} at $\tan\beta \sim 5.5$, at which point we obtain $N_{SD} \sim 3$. From these and other slightly less marginal cases we find the rough rule of thumb that this discovery technique achieves a $N_{SD} = 5$ signal so long as $B(t \to H^+ b) \gtrsim 0.003$.

D. Impact of eliminating b-tagging requirement

The b-tag requirement was included in the previous analysis to ensure that all non-$t\bar{t}$ backgrounds are negligible. Even higher N_{SD} values are potentially achievable in the absence of any b tagging. This could be of particular importance in the regions where $B(t \to H^+ b)$ is small, and the one-b-tag requirement leads to a marginal value of N_{SD}. In Fig. 8 we compare results with and without b tagging, for both $p_T(\pi) > 50$ GeV and $p_T(\pi) > 100$ GeV (the upper and lower curves of each pair of curves, re-

spectively).

In Table II we focus on an example in the region of $\tan\beta \sim 6$ where N_{SD} is minimum. We have assumed that the WW l-τ events are the only background to the WH l-τ events. As we have discussed, this is certainly the case when a b-quark jet is tagged. However, a very thorough analysis of several additional potential backgrounds would be required before one could claim that the level of backgrounds remaining is small in the absence of any b tagging. Potential new backgrounds include W+jets backgrounds of *all* types and $\tau\bar{\tau}$+jets. The former might be adequately suppressed by the high-p_T isolated pion requirement.[8] The latter could produce a high-p_T isolated pion (and lepton) if the initial τ's are sufficiently energetic, but would not automatically have associated jets with high p_T. Even when b tagging is not employed, the b and $\bar{b}$ jets automatically present in the $t\bar{t}$ events tend to have high p_T. In contrast, cuts that required high jet activity would not be easily satisfied by either the W+jets or $\tau\bar{\tau}$+jets backgrounds. Thus, it may be worth pursuing the no-b-tag option. But it must certainly be emphasized that a detailed study would be required to determine if, for instance, the 2061 WH l-τ events with no b tag and $p_T(\pi) > 50$ GeV would constitute a reliable signal in the presence of these backgrounds.

E. Indirect determination of the charged-Higgs-boson mass

While it is clear from the above results that the $\tau\nu \to \pi\nu\nu$ decays mode of the charged Higgs boson leads to a level of universality violation that is generally easily detected, the neutrinos emerging from the Higgs-boson and τ decays would seem to make a determination of $m_{H^\pm}$ impossible. In this section we shall demonstrate that there are distributions that allow a crude determination of the charged-Higgs-boson mass. In particular, we will define two mass variables that exhibit peaks which can reflect the charged-Higgs-boson mass rather directly.

First, we should not forget that the number of extra $\tau\nu$ events observed, $N_{l\tau}^{WH}$, will itself provide strong constraints. This is because the l-l and other channels will allow a very accurate determination of m_t. For a fixed choice of $\tan\beta$, the observed value of $N_{l\tau}^{WH}$ will then only be achieved for a fairly well-determined value of $m_{H^\pm}$. But, since we do not know in advance the value of $\tan\beta$ (and, hence, the $t \to H^+ b$ and $H^+ \to \tau\nu$ branching ratios), this constraint will only determine an allowed set of correlated m_{H^+} and $\tan\beta$ values.

As seen from Fig. 4, for a known m_t value, the b-quark spectrum from $t \to H^+ b$ decay will reflect the value of m_{H^+}. However, because of the need for a minimum p_T in order to tag a b jet, and because of the fact that the $t \to W^+ b$ channel will, in general, contaminate the distribution, the shapes of the observable parts of the p_T^b spectra need not be strongly correlated with m_{H^+}. To illustrate the situation, we focus on $m_t = 150$ GeV and present in Fig. 10 the p_T spectra of the tagged b in which the b has been associated with the $\tau\nu$ side of the event by requiring that $(p_\pi + p_b)^2 < m_t^2$ and $(p_l + p_b)^2 > m_t^2$. Events in which the tagged b do not satisfy these two criteria are discarded. In this way, the only combinatoric background is that which arises from extra b quarks not associated with the primary t decays. From Fig. 10 we see that if $\tan\beta$ is such that $B(t \to H^+ b)$ is large, then as m_{H^+} is increased from low to moderate values the b-quark spectra show a significant softening (compare the $m_{H^+} = 75$ GeV and $m_{H^+} = 125$ GeV curves). However, once $B(t \to H^+ b)$ becomes small, either because m_{H^+} begins to approach the $t \to H^+ b$ threshold (i.e., $m_{H^+} \gtrsim 135$ GeV for the $m_t = 150$ GeV choice being considered), or, because $\tan\beta$ is near the $\tan\beta \sim 5.5$ dip in $B(t \to H^+ b)$, the b's from the $t \to W^+ b$ decays obscure those from $t \to H^+ b$ so as to wash out any clear differences in the b spectra shapes. Thus, if the p_T spectrum of the b jet has a *shape* like that expected for $t \to W^+ b$ decays, we can only conclude that either $\tan\beta$ is near the $\tan\beta \sim 5.5$ region or that m_{H^+} is fairly near to m_t. Of course, whatev-

TABLE II. An example of the number of events found with and without b tagging in $WWb\bar{b}$ and $WHb\bar{b}$ events where we have chosen $m_t = 150$ GeV and $m_{H^\pm} = 135$ GeV and $\tan\beta \simeq 6$. We have only calculated the background from the WW l-τ events in finding N_{SD}.

		With b tagging	No b tagging
$N_{l\tau}^{WH}$	$[p_T(\pi) > 50$ GeV$]$	409	2061
$N_{l\tau}^{WW}$	$[p_T(\pi) > 50$ GeV$]$	3949	14 852
$N_{l\tau}^{WH}$	$[p_T(\pi) > 100$ GeV$]$	135	656
$N_{l\tau}^{WW}$	$[p_T(\pi) > 100$ GeV$]$	668	2700
N_{SD}	$[p_T(\pi) > 50$ GeV$]$	6.2	15.8
N_{SD}	$[p_T(\pi) > 100$ GeV$]$	4.76	11.3

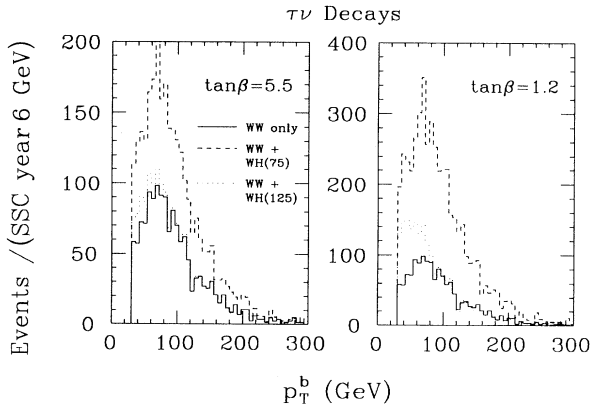

FIG. 10. The p_T spectra of a single tagged b jet from the $\tau\nu$ side of the event (using the criteria described in the text) are compared for the cases of $m_{H^+} = 75$ GeV (dashed curve) and $m_{H^+} = 125$ GeV (dotted curve). $WWb\bar{b}$ and $WHb\bar{b}$ events are combined as appropriate for $\tan\beta = 1.2$ and $\tan\beta = 5.5$. Also shown (solid curve) is the spectrum from WW events alone. We have taken $m_t = 150$ GeV and required $p_T(\pi) \geq 50$ GeV.

[8]As noted earlier, the probability for a QCD jet to look like an isolated π with $p_T(\pi) > 50$ GeV is about 0.1%.

er information we do glean from the b-quark spectrum can be combined with the overall normalization constraint discussed in the previous paragraph to better determine the best $\tan\beta$, m_{H^+} value(s).

We turn now to the mass variables. Let us suppose that the charged Higgs boson emerges from $t\to H^+b$, while the other side of the event provides the $\bar{t}\to W^-\bar{b}\to l^-\nu\bar{b}$ leptonic trigger. Our two mass variables are based on two distinct approximations to the top-quark momentum p_t. For both approximations we must identify the b jet associated with the $t\to H^+b$ decay. Experimentally, this means that we must adopt an algorithm (to be discussed below) for deciding whether the tagged b jet is that coming from the $t\to H^+b$ decay. Further, in constructing our approximations it is necessary to neglect the momentum carried by any jets that are radiated from the b and $\bar{b}$ and that also do not appear in the corresponding cluster as found in the ISAJET analysis. With this latter assumption, we may write

$$m_{H^+}^2=(p_t-p_b)^2=m_t^2+m_b^2-2p_t\cdot p_b \ . \tag{10}$$

(1) For the first approximation to the top-quark momentum p_t we note that $p_t=-p_{\bar{t}}-\sum' p_j$, where $\sum' p_j$ is the sum over all jets except those from the t and $\bar{t}$ decay products. Neglecting jets radiated from the $\bar{b}$, we have $p_{\bar{t}}=p_{\bar{b}}+p_l+p_\nu$ and, hence,

$$\begin{aligned} p_t&=-(p_{\bar{b}}+p_l+p_\nu)-\sum' p_j \\ &=-(p_{\rm tot}+p_\nu-p_b-p_\pi) \ , \end{aligned} \tag{11}$$

where $p_{\rm tot}$ is the sum of the momenta of all final-state particles (other than neutrinos). This approximation to p_t consists of determining $p_{\rm tot}$ by summing only over the four-momenta of the final-state clusters found in the $|\eta|<5$ region by the ISAJET simulation (including the trigger l and the π), and neglecting p_ν in Eq. (11). The escape of particles down the beam hole ($|\eta|>5$) implies that there will be a small error in the transverse component of $p_{\rm tot}$ and, of course, that the longitudinal component of $p_{\rm tot}$ cannot be determined in this way with any significant accuracy. Thus, we employ only transverse energies and momenta in computing $p_t\cdot p_b$ in Eq. (10), and find

$$m_{H^+}^2\sim s_{tb}\equiv m_t^2+m_b^2-2E_b^TE_t^T+2\mathbf{p}_t^T\cdot\mathbf{p}_b^T \ , \tag{12}$$

where $\mathbf{p}_t^T\simeq-(\mathbf{p}_{\rm tot}-\mathbf{p}_b-\mathbf{p}_\pi)^T$, $E_t^T=\sqrt{m_t^2+(p_t^T)^2}$, and $E_b^T=\sqrt{m_b^2+(p_b^T)^2}$.

(2) Our second approximation to p_t is obtained by neglecting the neutrinos that emerge in the $H^+\to\pi\nu\bar{\nu}$ decay [the strong $p_T(\pi)$ cut tends to suppress their energies, thereby reducing the error from this approximation]. Thus, we take

$$p_t\sim p_b+p_\pi \ , \tag{13}$$

which upon substitution into Eq. (10) yields

$$m_{H^+}^2\sim s_{\pi b}\equiv m_t^2-m_b^2-2p_\pi\cdot p_b \ . \tag{14}$$

[Note that had we not substituted the on-mass-shell value of p_t^2 is obtaining Eq. (10) prior to the substitution of Eq. (13) we would have simply obtained the triviality $s_{\pi b}=m_\pi^2$.] Since both approximations rely to some extent on the neutrinos from the H^+ decay being soft, it is not surprising that for adequate event samples these mass variables are best able to distinguish between different H^+ masses for the larger of the two $p_T(\pi)$ cuts studied.

Of course, an important ingredient in our procedure is the specification of which tagged b jet is to be employed in computing values for s_{tb} and $s_{\pi b}$. To reduce combinatoric background, we need to impose constraints such that a tagged b that is used has a high probability of coming from the $t\to H^+b$ decay.[9] If both $(p_\pi+p_b)^2<m_t^2$ and $(p_l+p_b)^2>m_t^2$ are satisfied, we follow the above outlined determination of s_{tb} and $s_{\pi b}$. If either criteria is not satisfied, then the event is discarded.[10] With these requirements imposed simultaneously, there is a high probability that the b jet is properly identified, the only background being that arising from extra b jets produced in ISAJET that came from neither t decay.

We can now illustrate the results obtained using s_{tb} and $s_{\pi b}$. Our plots will be in terms of $M_{tb}\equiv\sqrt{s_{tb}}$ and $M_{\pi b}\equiv\sqrt{s_{\pi b}}$. Events of the WW background type are added to those of the WH type with the appropriate weight as determined by $\tan\beta$. The net distribution is then plotted. The event numbers are absolutely normalized to (event number)/(SSC year) (6 GeV). However, it is the differences in distribution shapes upon which we shall focus. We study various $\tan\beta$ and m_{H^+} cases at $m_t=150$ GeV. We have chosen to consider three unequally spaced values of m_{H^+}: $m_{H^+}=75$, 105, and 125 GeV. We shall examine two representative $\tan\beta$ values: $\tan\beta=1.2$, where $N_{\rm SD}$ peaks, and $\tan\beta=5.5$, where $N_{\rm SD}$ is very near its minimum for all three m_{H^+} choices. A couple of generalities can be stated. In the case of the M_{tb} variable, the greatest significance for peak separation for the difficult $\tan\beta=5.5$ choice is obtained for the $p_T(\pi)>100$ GeV cut. For the cases where $B(t\to H^+b)$ is small, using $p_T(\pi)>50$ GeV allows significantly more events in the distributions, but the peak overlap increases substantially. For the $M_{\pi b}$ variable, the peak separation is always best for the $p_T(\pi)>100$ GeV cut.

In Fig. 11 we display M_{tb} distributions for $p_T(\pi)>100$ GeV, for the above-mentioned two $\tan\beta$ choices. We note that for the fairly optimal $\tan\beta=1.2$ choice there are significant peak separations between the three different mass choices, even though the separations are much smaller than the amount by which the different m_{H^+} masses are themselves separated. For $\tan\beta=5.5$ the $m_{H^+}=75$ and the $m_{H^+}=125$ GeV (and perhaps the $m_{H^+}=105$ GeV) distributions still look distinguishable, but the 105- and 125-GeV histograms look similar. Turn-

[9]This is not to say that the b jet from the $\bar{t}\to W^-\bar{b}$ decay does not appear as one of the reconstructed jet clusters.

[10]Of course, all of this is done at the detector level in terms of cluster momenta.

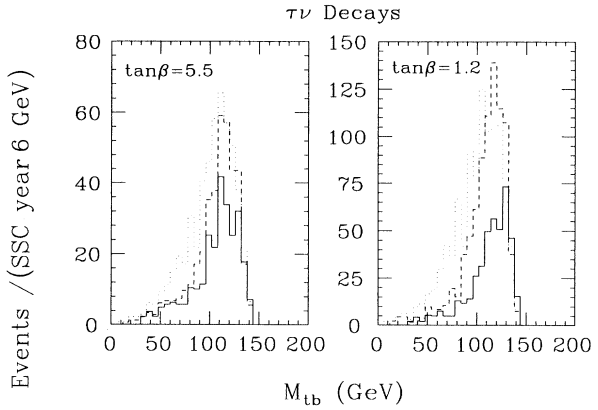

FIG. 11. Comparison of M_{tb} distributions for $m_{H^+}=75$ (dotted curve), 105 (dashed curve), and 125 GeV (solid curve) after requiring one b tag and $p_T(\pi)>100$ GeV. We have taken $m_t=150$ GeV and present results for $\tan\beta=1.2$ and $\tan\beta=5.5$.

ing to the $M_{\pi b}$ variable, we see from Fig. 12 that essentially the same remarks as for the M_{tb} variable again apply. The $M_{\pi b}$ variable leads to apparently narrower and more sharply defined peaks, but the differences in their mass discriminating powers are slight.

An interesting question is, to what extent are these distributions sensitive to the π, b, and jet resolutions? The results presented in Figs. 11 and 12 are those obtained with perfect resolution. We have compared the shapes of the mass peaks generated for WW and WH events, as incorporated into our figures, with those found after including resolutions similar to those of the SDC detector. Jets were smeared using a resolution of $70\%/\sqrt{E}+5\%$ and the pion momentum was smeared using $\Delta p/p=0.02\%\ p(\text{GeV})$. Although the smeared results were generated with fewer statistics, we found no significant change in the shapes of the mass distributions. We believe that this can be at least partly attributed to the fact that the M_{tb} and $M_{\pi b}$ mass variables are *ab initio* only approximate smeared-out reconstructions of m_{H^+}.

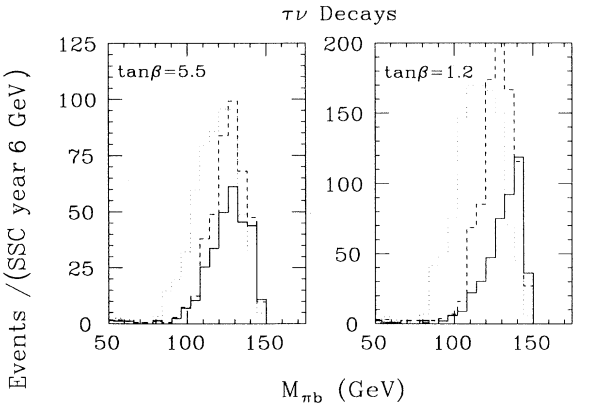

FIG. 12. Comparison of $M_{\pi b}$ distributions for $m_{H^+}=75$ (dotted curve), 105 (dashed curve), and 125 GeV (solid curve) after requiring one b tag and $p_T(\pi)>100$ GeV. We have taken $m_t=150$ GeV and present results for $\tan\beta=1.2$ and $\tan\beta=5.5$.

Since the peak separation and distribution shapes depend not only on m_{H^+} but also on $\tan\beta$, an iterative strategy to determining these two parameters is generally required. First, as described earlier, we can use the absolute value of $N_{l\tau}^{WH}$ to determine allowed correlated values of $\tan\beta$ and m_{H^+}. For example, when the $t\to H^+b$ branching ratio is not small (e.g., our $\tan\beta=1.2$ choice), $N_{l\tau}^{WH}$ depends primarily on $\tan\beta$ and can be used to make a first approximate determination of the latter. Comparison between the predicted and observed mass distribution shapes in either M_{tb} or $M_{\pi b}$ can then be used to make a final determination of m_{H^+} and a final adjustment to the best value of $\tan\beta$. The above results suggest that we can ultimately distinguish between m_{H^+} masses separated by about 20 GeV if $\tan\beta$ is not in the unfavorable dip region around $\tan\beta\sim5.5$.

F. $\tau\nu$ conclusions

Violation of l-τ universality provides a robust means for detecting the charged Higgs boson of a model II two-doublet Higgs sector that is sufficiently light to appear in top decays, throughout the theoretically preferred region of parameter space, $\tan\beta\gtrsim0.5$, so long as $B(t\to H^+b)\gtrsim0.003$. For low values of m_t (~100 GeV), this means that one can probe to within a few GeV of threshold for $t\to H^+b$. For large values of m_t (~200 GeV), a charged Higgs boson within about 10 GeV of m_t generally has $B(t\to H^+b)\gtrsim0.003$ (for $\tan\beta$ away from the $\tan\beta=5.5$ dip region) and can be detected.

While an absolutely direct determination of the H^+ mass from the position of a mass variable peak is not possible in the $\tau\nu$ decay mode, we have seen that the two approximate mass variables M_{tb} and $M_{\pi b}$ exhibit peaks and distributions that are sensitive to m_{H^+}. When $\tan\beta$ is such that $B(t\to H^+b)$ is large, a difference between distributions for two different m_{H^+} values separated by as little as 20–25 GeV may be observed. But when $B(t\to H^+b)$ is below 1%, a clear difference in distribution shapes occurs only for a m_{H^+} mass difference $\gtrsim35$–40 GeV. Further, for small $B(t\to H^+b)$, the spectrum of the tagged b jet associated with the $\tau\nu$ side of the event is dominated by the W decays and will not provide much additional information. Only a precise determination of the $N_{l\tau}^{WH}$ event excess will indicate how close to the $t\to H^+b$ threshold the H^+ mass is.

It is useful to remark briefly on what happens in a two-doublet model of type I. As noted in several earlier footnotes, the $\tau\nu$ branching ratio is independent of $\tan\beta$, while $B(t\to H^+b)$ falls rapidly in the $\tan\beta\gtrsim1$ region. Thus, use of the universality violation signal will not be possible at large $\tan\beta$ (and, indeed, all modes will fail for large enough $\tan\beta$). A more detailed computation of $N_{\rm SD}$ in this model (using the same cuts and efficiencies, etc. as employed for model II) shows that detection of the $H^\pm$ in model I is possible for $0.1\lesssim\tan\beta\lesssim2$–10, depending upon the choice of m_{H^+} and m_t. As in the case of model II, it is possible to give a rough rule of thumb: detection of a model I charged Higgs boson is possible using its $\tau\nu$ de-

cays, with a b tag and a cut of $p_T(\pi) > 50$ GeV, whenever $B(t \to H^+ b) \gtrsim 0.01$.

Returning now to the preferred model II case, it is clear that for small values of $\tan\beta$ ($\lesssim 0.5$), where $B(H^+ \to \tau\nu)$ becomes small, we must employ the $H^+ \to c\bar{s}$ decay mode, to which we now turn.

III. METHOD 2: SEARCH FOR $H^+ \to c\bar{s}$

In this section, we develop a technique for detecting a charged Higgs boson that decays to $c\bar{s}$. We focus entirely upon the $m_t = 150$ GeV, $m_{H^\pm} = 125$ GeV case. However, the procedures developed are easily extrapolated to other mass choices [2]. The ISAJET Monte Carlo is used to generate two samples of $t\bar{t}$ events with decays to $W^- H^+ b\bar{b}$ and $W^- W^+ b\bar{b}$. The H^+ is then decayed to $c\bar{s}$ and the W^+ to $u\bar{d}$ or $c\bar{s}$. The $W^- \to l\nu$ decay is used to provide the leptonic trigger for the events of interest. Detector simulation is performed using the detector model described in the recent SDC TDR [3]. Jets were reconstructed using the clustering algorithm described in Sec. 3.1.1 of that proposal, with a cone size $R = 0.4$ in the region $|\eta| < 2.5$. Some of the details of our procedures were developed for determining the mass of the top quark using its three-jet decays and are described in depth in the SDC TDR [3]; they will be referenced as needed here.

A. Event selection and efficiencies

Events are selected in which the t and $\bar{t}$ are produced recoiling opposite one another with high transverse momentum. Event rates and efficiencies for the cuts described below are listed in Table III. For the trigger we require an isolated electron or muon with $p_T > 40$ GeV and $|\eta| < 2.5$, using the isolation requirement described previously. As seen earlier for the $\tau\nu$ mode study, the efficiency for tagging the lepton is identical for the $W^- H^+$ and $W^- W^+$ events. Next, we require that at least three jets are reconstructed, each with $p_T > 30$ GeV (before the correction to be described below) in the opposite hemisphere to the lepton ($\Delta\phi > 90°$). One of these jets must be a b jet within $|\eta| < 2$, which is tagged via a secondary vertex.

As shown earlier in Fig. 4, the p_T spectrum of the b jet is much softer for the charged-Higgs-boson decay than for the W decay when the mass difference assumed between the H^+ and the t is small, resulting in a lower efficiency to observe the b jet. A second difference, illustrated in Fig. 13, is that the two jets from the H^+ decay are typically further apart than those from the W^+ decay in the WW events (see Fig. 13). This difference arises partly because of the higher H^+ mass, but also because of the W^+ polarization in the $t \to W^+ b$ decay.

TABLE III. Summary of event samples and efficiencies for the event selection in $WWb\bar{b}$ and $WHb\bar{b}$ events for $m_t = 150$ GeV and $m_{H^\pm} = 125$ GeV.

	$WWb\bar{b}$ events	$WHb\bar{b}$ events
$\sigma(t\bar{t})$	12 nb	
$N_{t\bar{t}}$	1.2×10^8	
Branching ratio	$\frac{8}{27}$	$\frac{4}{9}B(H^+ \to c\bar{s})$
Lepton, geometric	0.43	0.43
Lepton identification, isolation	0.85	0.85
b jet, geometric	0.51	0.30
b-jet vertex tag	0.30	0.30
$N(p_T(3\text{ jet})) > 200$ GeV	1.6×10^5	$(1.3\times10^5)B(H^+ \to c\bar{s})$

The combinatoric background can be reduced by requiring the transverse momentum of the three-jet system to be large, so that the three jets are near to one another and tend to be separated from jets arising either from initial-state radiation or from the other t decay. In what follows, we choose the minimum three-jet p_T to be 200 GeV, resulting in 158 000 [126 000 $B(H^+ \to c\bar{s})$] t-candidate three-jet combinations per nominal SSC year, assuming only WW (WH) decays.

B. Invariant-mass distributions

The invariant-mass distributions for the two jets (not including the b jet) in WW events and WH events are plotted in Fig. 14, and the three-jet invariant-mass distributions are shown in Fig. 15. In both cases, a large invariant-mass peak for the W, H, or t is evident, and the combinatoric background is relatively small. Since the jet four-momenta have not been corrected for detector and out-of-cone effects, the peaks are at lower invariant mass than the actual particle masses (73.9 GeV for the W, 111.4 GeV for the H, and 134.1 GeV for the t).

In general, the jet cluster momenta need to be corrected for three basic effects: (1) nonlinearity and other losses (cracks, neutrinos, leakage) that cause the energy deposited in the cluster to be measured low; (ii) energy from the jet that goes outside the cluster cone (either produced at large angles or bent by the magnetic field); and (iii) energy entering the cone from the underlying event or background events. For the cone size used, the predominant effect for these jets is calorimeter nonlinearity to low-momentum hadrons. In subsequent plots, an average correction factor has been applied as explained in the

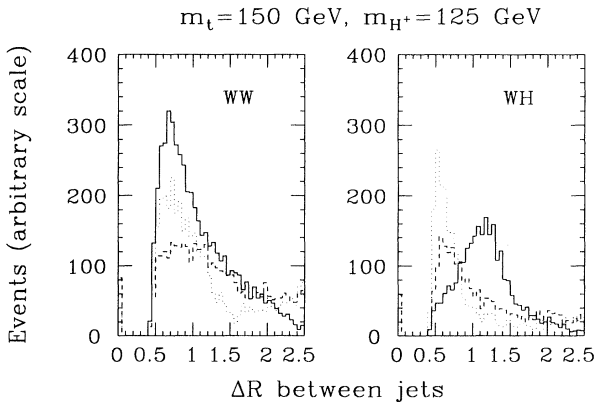

FIG. 13. Distance in η-ϕ space between the three jets (a) in $WWb\bar{b}$ events and (b) in $WHb\bar{b}$ events. The solid histogram is the distance between the two non-b jets, and the dashed (dotted) histogram is the distance between the lower-p_T jet (higher-p_T jet) and the b jet.

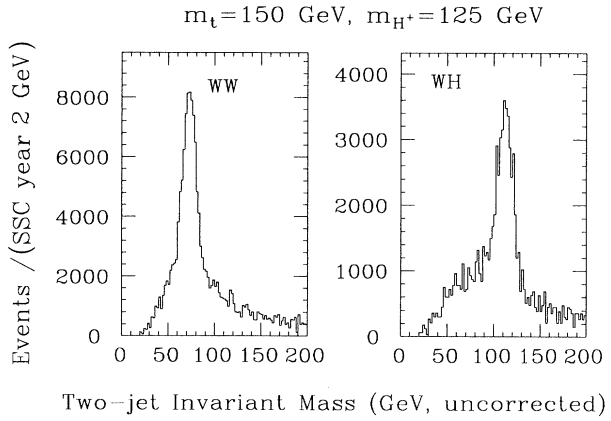

FIG. 14. Measured (uncorrected) two-jet invariant-mass distribution for a sample of (a) $t\bar{t}\rightarrow WWb\bar{b}$ events and (b) $t\bar{t}\rightarrow WHb\bar{b}$ events. Neither jet is the tagged b jet. Normalization is that appropriate if the top quark decays purely to the indicated channel.

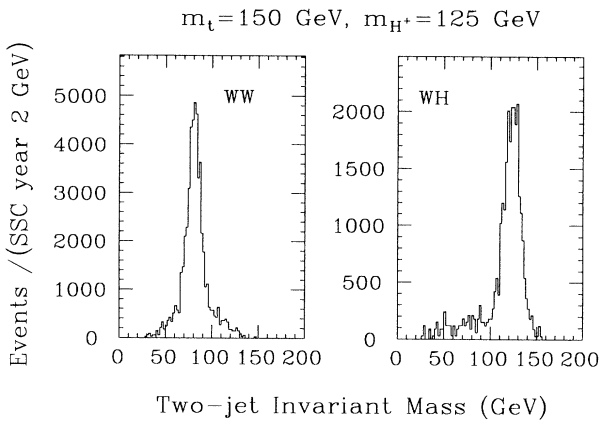

FIG. 16. Corrected two-jet mass distribution for samples of (a) $t\bar{t}\rightarrow WWb\bar{b}$ events and (b) $t\bar{t}\rightarrow WHb\bar{b}$ events. In this plot the three-jet invariant mass is required to be consistent with the t mass, or $120 < M(3\text{ jet}) < 150$ GeV (uncorrected).

SDC TDR [3]. To reduce the background further to the two-jet invariant-mass distribution, we require that the corrected three-jet invariant mass be in the range $135 < M(3\text{ jet}) < 165$ GeV. The two-jet mass distributions after this cut are shown in Fig. 16. With the jet four-momenta corrected, the W mass peak appears at 80.5 GeV (the generated mass is 80.0 GeV) with a width of 7.5 GeV, and the H mass peak appears at 123.3 GeV with a width of 8.5 GeV. Since the momentum rescaling alone yields masses very near the correct value, it would seem that the effects coming from the underlying event and from energy outside the jet cone either are small or cancel each other out.

Likewise, if we require the two-jet invariant mass in the WW case to be in the range 65–95 GeV, the three-jet invariant mass (see Fig. 17) shows almost no background. And if we require the two-jet invariant mass in the WH case to be in the range 110–140 GeV, the three-jet invariant mass plotted for this case in Fig. 17 shows almost no background. The measured t invariant masses in the WW and WH modes are 147.9 and 148.2 GeV, each with a width slightly below 9 GeV. The statistical precision for the t invariant mass for 1 SSC yr would be less than 40 MeV. Systematic uncertainties for this measurement will be dominated by the jet energy scale (calorimeter calibration, nonlinearity, energy outside the jet cone, and underlying event or pileup). Much of this uncertainty can be reduced using the W mass constraint, with the remaining uncertainty due to the b-jet measurement. Another method to reduce the uncertainty would be to use a track-by-track jet correction for nonlinearity; in the Collider Detector at Fermilab (CDF) Collaboration this was shown to reduce systematic uncertainty and also to improve the jet energy resolution by 10–15 % [10].

C. Determination of statistical significance of mass peaks

To determine the statistical significance of the $H^{\pm}$ and $W^{\pm}$ mass peaks for a particular branching fraction

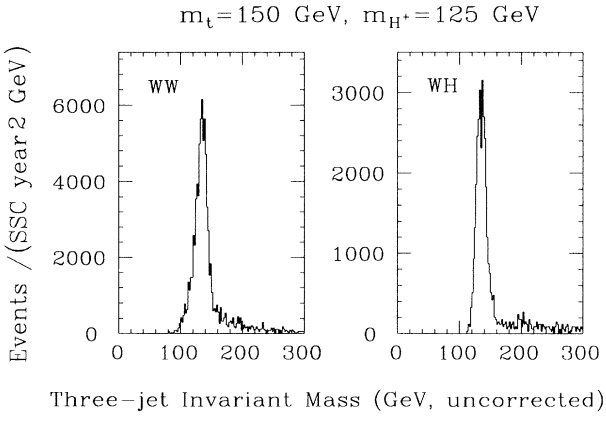

FIG. 15. Measured (uncorrected) three-jet invariant-mass distribution for a sample of (a) $t\bar{t}\rightarrow WWb\bar{b}$ events and (b) $t\bar{t}\rightarrow WHb\bar{b}$ events.

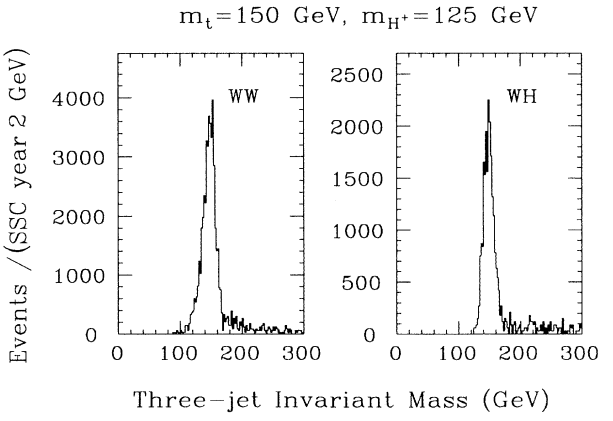

FIG. 17. Corrected three-jet mass distribution for samples of (a) $t\bar{t}\rightarrow WWb\bar{b}$ events and (b) $t\bar{t}\rightarrow WHb\bar{b}$ events. In this plot the two-jet invariant mass is required to be consistent with the W or H^+ mass.

$B(t \to H^+ b)$, the ideal technique would be to fit the dijet invariant-mass distribution obtained from the data to the distributions obtained using a Monte Carlo simulation that produces both WW and WH events (with a W or H decaying to jets). This will give a best value for the fraction of WH events in the data (or a limit on the amount of WH present). This value is determined by $B(t \to bH^+)$ and $B(H^+ \to c\bar{s})$; hence using Figs. 1 and 2 one can determine the best value of $\tan\beta$. As an example, the two-jet invariant-mass distributions obtained after imposing the selection criteria (and efficiencies) are shown in Fig. 18 for the particular cases of $\tan\beta=0.4$ [yielding $B_H=0.42$ and $B(H^+ \to c\bar{s})=0.98$] and $\tan\beta=1.0$ [yielding $B_H=0.096$ and $B(H^+ \to c\bar{s})=0.59$]. For $\tan\beta=0.4$, the $W^\pm$ and $H^\pm$ mass peaks are both very prominent, and discovery of the $H^\pm$ is clearly possible. The $\tan\beta=1.0$ case is somewhat marginal, since the combinatoric background would have to be well understood to claim a signal. The statistical significance is quite high since the statistical errors are small; however, in this case we would prefer to rely on method 1 ($H^+ \to \tau\nu$), which is effective down to $\tan\beta=0.5$.

Since our mass assumptions yield two reasonably well separated mass peaks, we have adopted a simple technique to roughly estimate the statistical significance of each peak. We consider the number of events in the two intervals $65 < M_{jj} < 95$ GeV (W interval) and $110 < M_{jj} < 140$ GeV (H interval). The background beneath the H peak has a contribution from both WW and WH events. Unlike the case in the previous study [2], the shapes of the background beneath the peaks in the WW and WH events are not too similar. We have estimated the level of background under the H peak in WH events by using a smooth curve overlapping each histogram on both edges of the H interval. This estimate is good to about 10%. The signal in the $H^\pm$ peak is then the number of events in the $H^\pm$ interval minus the estimated background. We follow the converse procedure in determining the number of events in the $W^\pm$ peak. For the two mass intervals, the estimated ratios of signal and of background events to the number of events passing the trigger, and event selection requirements in the WW and WH processes are shown in Table IV. In obtaining the results of this table, we have also required that the corrected three-jet invariant mass be in the range $135 < M(3\text{ jet}) < 165$ GeV.

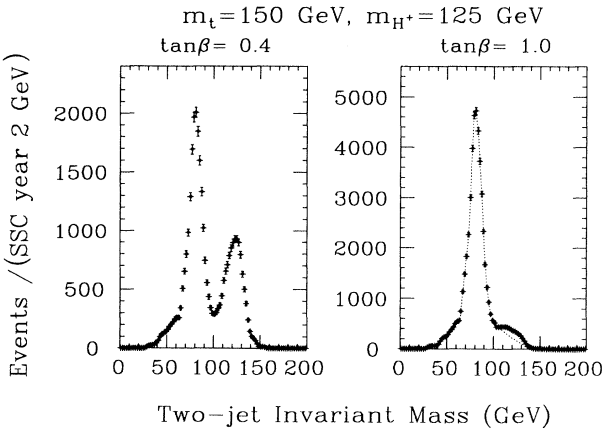

FIG. 18. Two-jet invariant-mass plot, after two-jet selection criteria are imposed, for the cases of (a) $\tan\beta=0.4$ and (b) $\tan\beta=1.0$. The plot is normalized to 1 SSC yr of running. The dotted curve in (b) indicates the background determined as described in the text. The three-jet mass cut in the vicinity of m_t has not been imposed. The error bars shown correspond to the statistics for 1 SSC yr.

To quantify the statistical significance of the $H^\pm$ and $W^\pm$ mass peaks, we plot the number of standard deviations above background as a function of $\tan\beta$:

$$N_{\rm SD} = \frac{N_{\rm above}}{\sqrt{N_{\rm above} + N_{\rm below}}} , \tag{15}$$

where $N_{\rm above}$ is the number of "excess" events appearing above the background curve and $N_{\rm below}$ is the number below the background curve in the two mass intervals mentioned above. The resulting values for $N_{\rm SD}$ are plotted as a function of $\tan\beta$ in Fig. 19. The highest $\tan\beta$ value for which we could discover the charged Higgs boson by this method would depend critically on understanding the shape of the combinatoric background. To be conservative we should claim to see a signal only when the shape of the distribution is clearly different from the background. Hence, we argue that method 2 is valid only for $\tan\beta < 1$.

D. Conclusions for $H^+ \to c\bar{s}$

As long as $\tan\beta < 1$, reconstruction of a clearly distinguishable H^+ mass peak is generally quite straightforward, and an accurate measurement of m_{H^+} is possible. For $\tan\beta \sim 1$ the product of the $t \to H^+ b$ and $H^+ \to c\bar{s}$ branching ratios is of order 0.05 in the $m_t=150$ GeV, $m_{H^+}=125$ GeV case explicitly studied. One can speculate that for other values of m_t and m_{H^+} the $c\bar{s}$ mass peak reconstruction technique will work when the product of branching ratios is larger than 0.05. However, such a simple rule may not work when m_{H^+} is near the threshold for $t \to H^+ b$ decay. Unlike the case of the $\tau\nu$ universality violation signal, the tagged b quark here must be determined to be the one from $t \to H^+ b$ in order to establish which two of the three jets from the t decay come from the H^+ (otherwise, we would have a large combinatoric background to our H^+ mass peak.) This b quark will be quite soft as the decay threshold is approached,

TABLE IV. Ratios of signal and background event numbers to total number of events passing trigger and event selection requirements. In particular, we required that the corrected three-jet invariant mass be in the range $135 < M(3\text{ jet}) < 165$ GeV.

	$WWb\bar{b}$ events	$WHb\bar{b}$ events
W peak signal	0.312	0
H peak signal	0	0.296
W peak bkgnd.	0.103	0.059
H peak bkgnd.	0.0185	0.055

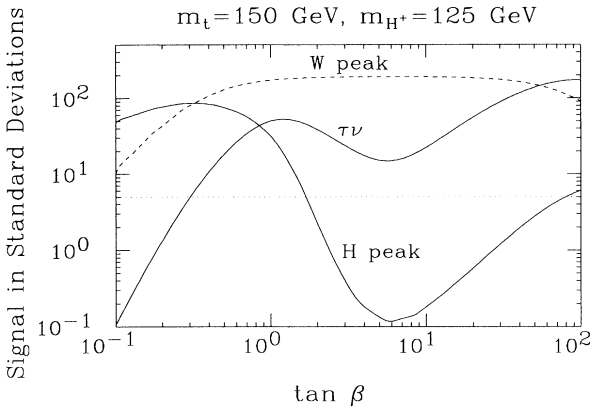

FIG. 19. The statistical significance, N_{SD} of Eq. (15), of the charged-Higgs and W-boson (dashed) peaks in the two-non-b-jet invariant-mass distribution (method 2) as a function of tanβ. Also shown is the statistical significance obtained using method 1 ($\tau\nu$). We assume 1 SSC yr of running and have taken $m_t = 150$ GeV and $m_{H^\pm} = 125$ GeV. The dotted line at 5 standard deviations indicates our assumed level for detection of the charged Higgs boson.

making tagging difficult. Thus, 0.05 should probably be regarded as the minimum value of $B(t \to H^+ b) \times B(H^+ \to c\bar{s})$ for which the $c\bar{s}$ peak reconstruction can work.

IV. CONCLUSIONS

We have examined charged-Higgs-boson production in $t\bar{t}$ events in which one t decays to $H^\pm b$ and the other to $W^\pm b$. This study was performed in the context of a two-Higgs-doublet model in which one Higgs doublet couples only to up-type quarks and the other only to down-type quarks and to leptons, but may apply in other contexts equally well. Discovery of the charged Higgs boson may be possible over the entire interesting range of parameter space.

Making use of a b-tagging capability, detection of $H^\pm$ for tan$\beta \gtrsim 0.5$ is possible through $H^+ \to \tau\nu$ decays, while for tan$\beta < 1$ the decays $H^+ \to c\bar{s}$ can be employed. In the $c\bar{s}$ mode, a direct determination of the H^+ mass is possible from a peak in the appropriate two-jet mass distribution. In the case of the $\tau\nu$ mode, we have found two mass variables that yield peaks and are generally sensitive to the H^+ mass for tanβ and m_{H^+} such that $B(t \to H^+ b)$ is not very small. Overall, the techniques developed illustrated the importance of efficiently identifying b-quark jets and τ's.

An important question is the extent to which these techniques remain viable if less than full luminosity is available (as might, for instance, be the case when the SSC first turns on). We have seen that at full luminosity ($L = 10$ fb^{-1}) the $\tau\nu$ technique is viable for tan$\beta \gtrsim 0.5$ if $B(t \to H^+ b) \gtrsim 0.003$, while for tan$\beta \lesssim 1$ the $c\bar{s}$ mode is viable if $B(t \to H^+ b) \gtrsim 0.05$. Were only $L = 1$ fb^{-1} available, then these branching-ratio criteria would need to be increased by about a factor of $\sqrt{10}$ in order to maintain the same level of significance for a signal. Typical of the impact of such a decrease in luminosity is the result obtained in the case of $m_t = 150$ GeV and $m_{H^+} = 125$ GeV illustrated in Fig. 19. If all the curves in this figure are lowered by a factor of $\sqrt{10}$ relative to the 5 standard deviation criterion line, one observes that $t \to H^+ b$ detection would continue to be possible at the 5σ level for any value of tanβ. In contrast, were only $L = 0.1$ fb^{-1} available, detection of the $t \to H^+ b$ decays would become extremely marginal or impossible for almost all tanβ values. In general, $t \to H^+ b$ detection will remain possible over much of m_{H^+}-tanβ parameter space if only $L = 1$ fb^{-1} is available, but would be severely impacted for $L \lesssim 0.1$ fb^{-1}.

ACKNOWLEDGMENTS

A portion of this work was completed during the U.C. Davis Workshop on Higgs Bosons/Electroweak Symmetry Breaking. J.F.G. would like to acknowledge the support and hospitality of the CERN theory group during the final stages of this project. B.H. wishes to acknowledge the support of the Texas National Research Laboratory Commission. Finally, we would like to acknowledge the important contributions to the earlier version of this study (Ref. [2]) from H. Haber, I. Hinchliffe, and H.-J. Trost. This work was supported by the Director, Office of Energy Research, Office of High Energy and Nuclear Physics, Division of High Energy Physics of the U.S. Department of Energy under Contract Nos. DE-AC03-76SF00098, DE-FG03-91ER40674, and DEFG03-91-ER40656, and by the National Science Foundation under Grant No. PHY-86-15529.

[1] For a review of Higgs bosons, see J. F. Gunion, H. E. Haber, G. Kane, and S. Dawson, *The Higgs Hunters Guide* (Addison Wesley, Reading, MA, 1990).

[2] R. M. Barnett, J. F. Gunion, H. E. Hager, I. Hinchliffe, B. Hubbard, and H.-J. Trost, Solenoidal Detector Collaboration Report No. SDC-90-141, 1990 (unpublished).

[3] Solenoidal Detector Collaboration Letter of Intent, SDC Report No. SDC-90-151, 1990 (unpublished); SDC Technical Design Report, SDC Report No. SDC-92-201, 1992 (unpublished).

[4] L^* Collaboration Letter of Intent, Report No. SSCL-SR-1154, 1990 (unpublished); EMPACT Collaboration Letter of Intent, Report No. SSCL-SR-1155, 1990 (unpublished); GEM Collaboration Letter of Intent, Report No. SSCL-SR-1184 (unpublished).

[5] Contributions in *Proceedings of the ECFA Large Hadron Collider Workshop,* Aachen, Germany, 1990, edited by G. Jarlskog and D. Rein (CERN Report No. 90-10, Geneva, Switzerland, 1990), Vol. II.

[6] R. M. Godbole and D. P. Roy, Phys. Rev. D **43**, 3640 (1991); D. P. Roy, Phys. Lett. B **283**, 403 (1992).

[7] Particle Data Group, K. Hikasa *et al.*, Phys. Rev. D **45**, S1 (1992).

[8] A. B. Wicklund, Solenoidal Detector Collaboration Re-

port No. SDC-91-051 (unpublished).
[9] B. Hubbard, Solenoidal Detector Collaboration Report No. SDC-90-031 (unpublished).
[10] B. Hubbard, Lawrence Berkeley Laboratory Report No. LBL-27687, 1989 (unpublished).
[11] Further study of the implications of this polarization difference has appeared in B. K. Bullock, K. Hagiwara, and A. D. Martin, Phys. Lett. B **273**, 501 (1991); Phys. Rev. Lett. **67**, 3055 (1991). See also D. P. Roy, Phys. Lett. B **277**, 183 (1992).
[12] I. Hinchliffe *et al.*, Solenoidal Detector Collaboration Report No. SDC-90-100, 1990 (unpublished).